Medical Image Analysis 12 (2008) 527–534

Contents lists available at ScienceDirect

Medical Image Analysis

journal homepage: www.elsevier.com/locate/media

# Real-time MR diffusion tensor and Q-ball imaging using Kalman filtering

Cyril Poupon *, Alexis Roche, Jessica Dubois, Jean-François Mangin, Fabrice Poupon

*CEA I2BM NeuroSpin – Bât. 145, Point Courrier 156, 91191 Gif-sur-Yvette, France*
*IFR49, 91191 Gif-sur-Yvette, France*

ARTICLE INFO

*Article history:*
Received 30 January 2008
Received in revised form 15 May 2008
Accepted 10 June 2008
Available online 19 June 2008

*Keywords:*
Diffusion-weighted MR imaging
DT model
Analytical Q-ball model
Optimized orientation distribution
Real-time processing

ABSTRACT

Diffusion magnetic resonance imaging (dMRI) has become an established research tool for the investigation of tissue structure and orientation. In this paper, we present a method for real-time processing of diffusion tensor and Q-ball imaging. The basic idea is to use Kalman filtering framework to fit either the linear tensor or Q-ball model. Because the Kalman filter is designed to be an incremental algorithm, it naturally enables updating the model estimate after the acquisition of any new diffusion-weighted volume. Processing diffusion models and maps during ongoing scans provides a new useful tool for clinicians, especially when it is not possible to predict how long a subject may remain still in the magnet. First, we introduce the general linear models corresponding to the two diffusion tensor and analytical Q-ball models of interest. Then, we present the Kalman filtering framework and we focus on the optimization of the diffusion orientation sets in order to speed up the convergence of the online processing. Last, we give some results on a healthy volunteer for the online tensor and the Q-ball model, and we make some comparisons with the conventional offline techniques used in the literature. We could achieve full real-time for diffusion tensor imaging and deferred time for Q-ball imaging, using a single workstation.


## 1. Introduction

Diffusion magnetic resonance (MR) imaging has become an established technique for inferring structural anisotropy of tissues and mapping the white matter connectivity of the human brain (LeBihan et al., 1986). The term diffusion refers to the Brownian motion of water molecules inside tissues that results from the thermal energy carried by these molecules. MR images can be sensitized to that physiological phenomenon from the application of a specific pair of well-known diffusion gradients together with a spin echo pulse sequence.

Technically, using diffusion imaging to infer the three dimensional displacement probability of water molecules requires the acquisition of a set of diffusion-sensitized images along different orientations of the space. Several mathematical models have been designed, becoming more and more complex over the last decade while attempting to make less and less assumptions. In this paper, we focus on both the diffusion tensor (DTI) model (historically the first) introduced by Basser et al. (1994) and the Q-ball model (QBI) introduced by Tuch (2002). Despite the huge amount of assumptions (unrestricted environment, structural homogeneity within voxels), the DTI model is still widely used because it can be used in a clinically acceptable time (a few minutes for an entire brain coverage) and provides useful information to the clinicians about the average translational motion (apparent diffusion coefficient, ADC), the anisotropy of white matter structure (fractional anisotropy index, FA), and the direction encoded color map (RGB). Today, clinical studies of brain pathologies (either neurodegenerative or psychiatric) involve statistical analysis of ADC and FA maps. Q-ball belongs to the class of high angular resolution diffusion imaging (HARDI) models that aim at solving the partial voluming problem due to the existence of several putative populations of fibres within a voxel. Such models have been developed to address the inference of white matter connectivity mapping from the knowledge of local microstructural orientations of tissue (Callaghan, 1991; Tuch, 2002; Frank, 2002; Jansons and Alexander, 2003; Zhan et al., 2003; Liu et al., 2004; Alexander, 2005; Ozarslan and Mareci, 2003; Wedeen et al., 2005; Assaf and Basser, 2005; Anderson, 2005; Ozarslan et al., 2006; Hess et al., 2006; Tournier et al., 2007; Jian and Vemuri, 2007; Descoteaux et al., 2007).

Compared to DTI, QBI requires from five to ten times more diffusion gradient orientations with a higher *b*-value and therefore cannot be considered as reliable for clinical use for many reasons. First, clinical protocols generally involve different MR acquisitions (T1, T2, BOLD) limitating the time allocated to diffusion imaging. Second, the patient may move severely during the acquisition (a frequent situation for patients impaired with Huntington disease, Parkinson disease, schizophrenia), hence increasing the risk of aborting the scanning. The same problem arises for studies

* Corresponding author. Address: CEA I2BM NeuroSpin – Bât. 145, Point Courrier 156, 91191 Gif-sur-Yvette, France. Tel.: +33 1 69 08 77 76; fax: +33 1 69 08 79 80.
*E-mail address:* cyril.poupon@cea.fr (C. Poupon).
*URL:* http://brainvisa.info (C. Poupon).

1361-8415/$ - see front matter © 2008 Elsevier B.V. All rights reserved.
doi:10.1016/j.media.2008.06.004

involving newborns who cannot be sedated: generally, less than 75% of the subjects can be exploited because they often wake up inside the magnet, due to the level of noise. Or the patient can be more cooperative than hypothesized first and it's worth starting with a high *b*-value DTI scan and continuing with a QBI scan if the patient remains still.

This paper addresses the feasibility of real-time DTI and QBI processing for displaying reconstructed associated maps during an ongoing scan. This will make it possible to start the scan estimating both models, to cancel the acquisition at any time, or to sustain the scanning when the subject is still in the magnet. If the scanning is stopped after too few diffusion gradient orientations, none of the model is exploitable. Then, according to the acquired number of orientations, either DTI model, QBI model or both can be obtained. To our knowledge, real-time processing was previously addressed for BOLD functional imaging (Roche et al., 2004) and EEG-fMRI fusion (Deneux and Faugeras, 2006), but has never been proposed for diffusion imaging.

DTI and QBI models can be expressed in the light of the general linear model framework (GLM) assuming a white noise model. Using the GLM model does not insure the positivity of the tensor model, and may not lead to correct Q-balls when negative diffusivity profiles occur, due to low SNR. However, the GLM model is convenient when employing incremental frameworks. Among available techniques for solving least-squares linear regression models, the Kalman filter provides an appropriate answer to the real-time requirement, as it is an incremental solver. After the acquisition of the entire volume for each diffusion gradient orientation, this filter can update DTI and QBI maps, provide variance of the estimate and can deliver an immediate feedback to the clinician or to the expert in cognitive neurosciences.

After introducing the linear models for DTI and QBI in Section 2, we describe the Kalman filter-based algorithm implemented in Section 3. Then we focus on the optimization of the diffusion gradient orientation set in Section 4. In Section 5, we give a setup of the real-time protocol used and we illustrate the technique using DTI and QBI MR data, before concluding.

## 2. Model fitting formulation

Let us consider the vector $\vec{m} = [m_1, \ldots, m_N]$, acquired during the acquisition corresponding to the diffusion-sensitized signal measured with the different diffusion gradient orientations at a given voxel in the scanned volume. The gradient orientations $\mathbf{o}_i$ are indexed by $i$ corresponding to the time rank during the acquisition and are numbered from 1 to $N$. The choice of the orientation set will be discussed later in Section 4. The magnitude of the sensitization is given by the $b$-value in s/mm$^2$. We also define $m_0$ corresponding to the unweighted signal measured with diffusion gradients off.

### 2.1. Tensor general linear model

The DT model states that the diffusion of water molecules can be considered as free, yielding a Gaussian probability density function characterized by a second order tensor **D**. The signal attenuation observed when applying a diffusion gradient along the normalized direction $\mathbf{o} = [o_x, o_y, o_z]^T$ of the space and with sensitization $b$ is exponential (Stejskal and Tanner, 1965):

$$m = m_0 e^{-b\mathbf{o}^T\mathbf{D}\mathbf{o}} + \mu \quad (1)$$

where $\mu$ represent the acquisition noise that usually follows a Rician distribution (Sijbers et al., 1998; Nowak, 1999). Taking the natural logarithm of this attenuation, we easily obtain the general linear model:

$$\mathbf{y} = \mathbf{B}\mathbf{d} + \epsilon \quad (2)$$

where we define the measured vector of attenuations $\mathbf{y} = [y_1, \ldots, y_N]^T$, with $y_i = \log(m_0/m_i)$ and $\mathbf{d} = [D_{xx}, D_{xy}, D_{xz}, D_{yy}, D_{yz}, D_{zz}]^T$ being the vector of the six unknown coefficients of the diffusion tensor. **B** is a $N \times 6$ matrix called the diffusion-sensitization matrix, built from $N$ rows $\mathbf{b}_1, \ldots, \mathbf{b}_N$ depending only on the diffusion gradient settings (Eq. (3)):

$$\mathbf{b_i} = b_i[o_{x,i}^2, 2o_{x,i}o_{y,i}, 2o_{x,i}o_{z,i}, o_{y,i}^2, 2o_{y,i}o_{z,i}, o_{z,i}^2] \quad (3)$$

$\epsilon$is the $N \times 1$ vector of errors $\epsilon_i = -\ln(1 + \mu e^{b_i \mathbf{o}_i^T \mathbf{D} \mathbf{o}_i}/m_0) \approx -\mu e^{b_i \mathbf{o}_i^T \mathbf{D} \mathbf{o}_i}/m_0$. Theoretically, the noise model depends on the unknowns as well as on the Rician noise $\mu$, but we assume it is not far from a Gaussian distribution. Studying the true distribution of the noise must be done, but it is not the purpose of this paper that deals with the real-time aspect of the algorithm. Moreover, the $b$-value used along with DT acquisition protocols remains usually lower than $1500 s/mm^2$, yielding a signal to noise ratio (SNR) greater than 10. When the SNR of an image remains higher than a typical value of 4, the Rician distribution can be assimilated to a Gaussian distribution without any loss of precision.

### 2.2. Analytical Q-ball general linear model

The Q-ball model states that the orientation distribution function (ODF) $\psi(\mathbf{o}) = \int_0^\infty p(r\mathbf{o})dr$ that gives the likelihood of having diffusion along orientation **o** can be obtained by sampling a sphere in Q-space (Tuch, 2002) which radius is set up by a high $b$-value (typically greater than 3000 s/mm$^2$) with a huge number of gradient orientations (from 160 to 500 according to the literature). A good approximation of the ODF was proposed by Tuch using the Funk–Radon transform (FRT). In order to obtain $\psi(\mathbf{o}_i)$, the FRT integrates the MR signal along the equator of the given orientation $\mathbf{o}_i$.

A first linear model of the FRT has been published in Tuch (2004) corresponding to the raw algorithm. This algorithm provides a linear relationship between the vector of magnetization acquired over the spherical shell in Q-space, and the vector of probabilities of the orientations over the sphere in the image space. Due to the large dimensions of the associated reconstruction matrix, the processing time may become very long, thus making the Q-ball model unexploitable in real-time.

More recently, Descoteaux proposed an elegant analytical reformulation of the FRT using the Funk–Hecke theorem for decomposing the ODF onto a symmetric, orthonormal and real spherical harmonics basis. The reader is invited to read Descoteaux et al. (2007) for the full details about the method as we will only briefly describe this development. Compared to numerical QBI, the analytical QBI reconstruction is faster, more robust to noise, and requires less gradient directions for stable reconstruction. Most information is contained in harmonic order 6 or less, with a large majority for lowest orders, providing an efficient data compression of the ODF information. Similar results were also described in Anderson (2005) and Hess et al. (2006).

Decomposing the diffusion signal onto a basis of spherical harmonics (SH) is quite natural since the acquisition is performed on a spherical shell and because the original Q-ball model is obtained from the FRT that uses spherical coordinates. However, as the diffusion signal is supposed to be real and symmetric, a modified real and symmetric SH basis is used (Eq. (4)). $\theta$ and $\phi$ represent the colatitude and the azimuth respectively of the unit vector **o** taken on the surface of a spherical shell in Q-space. $P_l^m(x)$ is the associated Legendre function of degree $l$ and phase factor $m$. The indices $k$ and $(l,m)$ are such that $k = (l^2 + l + 2)/2 + m$ and $-l \leqslant m \leqslant +l$,

$$Y_l^m(\theta,\phi) = \sqrt{\frac{2l+1}{4\pi}\frac{(l-m)!}{(l+m)!}}P_l^m(\cos\theta)e^{im\phi},$$

$$Y_k(\theta,\phi) = \begin{cases} \sqrt{2}\mathrm{Re}(Y_l^{|m|}(\theta,\phi)) & \text{if } -l \leqslant m < 0 \\ Y_l^m(\theta,\phi) & \text{if } m = 0 \\ (-1)^{m+1}\sqrt{2}\mathrm{Im}(Y_l^m(\theta,\phi)) & \text{if } 0 < m \leqslant l \end{cases} \quad (4)$$

A $N \times K$ matrix $\mathbf{B}$ corresponding to the discrete sampling of the diffusion signal along the $N$ diffusion gradient orientations $\mathbf{o}_i$ and taken onto the spherical shell at a given $b$-value can be associated to the orthogonal SH basis using the $K = (l+1)(l+2)/2$ first spherical harmonics (Eq. (5)):

$$\mathbf{B} = \begin{pmatrix} Y_1(\theta_1,\phi_1) & \cdots & Y_K(\theta_1,\phi_1) \\ \vdots & \ddots & \vdots \\ Y_1(\theta_N,\phi_N) & \cdots & Y_K(\theta_N,\phi_N) \end{pmatrix} \quad (5)$$

Let $\mathbf{c}^{\mathrm{DWI}} = [c_1,\ldots,c_K]^T$ be the $K \times 1$ vector of coefficients $c_k^{\mathrm{DWI}}$ of the spherical harmonics decomposition of the diffusion signal (Eq. (6)):

$$m(\theta,\phi) = \sum_{k=1}^{K} c_k^{\mathrm{DWI}} Y_k(\theta,\phi) \quad (6)$$

Descoteaux proposed a robust estimate of the vector $\mathbf{c}^{\mathrm{DWI}}$ using a Laplace–Beltrami regularization that decreases the occurence of negative peaks in the recomposed diffusion signal for high SH orders, though it cannot guarantee the absence of negative peaks (Eq. (7)). The Laplace–Beltrami operator corresponds to the Laplacian operator in spherical coordinates and is simply given by a $K \times K$ diagonal matrix $\mathbf{L}$ which elements are equal to $l(k)^2(l(k)+1)^2$. $\lambda$ is a regularization factor that controls the smoothing effect of the estimator,

$$\mathbf{c}^{\mathrm{DWI}} = (\mathbf{B}^{\mathrm{T}}\mathbf{B} + \lambda\mathbf{L})^{-1}\mathbf{B}^{\mathrm{T}}\mathbf{m} \quad (7)$$

Replacing the diffusion signal by its decomposition on the modified SH basis in the original Funk–Radon transform and using the Funk–Hecke theorem, Descoteaux demonstrated that the decomposition $\mathbf{c}^{\mathrm{ODF}}$ of the ODF on the same SH basis can be obtained analytically from the reconstruction Eq. ((8)), where $\mathbf{P}$ is the $K \times K$ Funk–Hecke diagonal matrix with elements $P_{kk} = 2\pi P_{l(k)}(0)$ ($P_{l(k)}(x)$ is the associated Legendre function of degree $l(k)$),

$$\mathbf{c}^{\mathrm{ODF}} = \mathbf{P}\mathbf{c}^{\mathrm{DWI}} \quad (8)$$

From the knowledge of the decomposition $\mathbf{c}^{\mathrm{ODF}}$, we can obtain the ODF value for any orientation $\mathbf{o}$ calculating the composition (9):

$$\psi(\mathbf{o}) = \sum_{k=1}^{N} c_k^{\mathrm{ODF}} Y_k(\theta(\mathbf{o}),\phi(\mathbf{o})) \quad (9)$$

One of the main advantages of this analytical reconstruction of the Q-ball model comes from the simple input parameters used to control the algorithm: the SH order $K$ tune up the level of details allowed in the ODFs and the regularization factor $\lambda$ controls the level of smoothness of the ODFs while preventing the apparition of negative peaks. Further investigation must be done concerning this factor in order to understand accurately its role, compared to the regularized scheme proposed by Tournier et al. (2007).

Eq. (8) can easily be reversed to get the equation of the equivalent general linear model (10):

$$\mathbf{m} = \mathbf{B}^{+}\mathbf{c}^{\mathrm{ODF}} + \epsilon \quad \text{with} \quad \mathbf{B}^{+} = (\mathbf{P}(\mathbf{B}^{\mathrm{T}}\mathbf{B} + \lambda\mathbf{L})^{-1}\mathbf{B}^{\mathrm{T}})^{\dagger} \quad (10)$$

where $\epsilon$ is the vector of Rician acquisition noise that we assume to be Gaussian in order to stay in the ordinary linear least-square framework. The $()^{\dagger}$ stands for the Moore–Penrose pseudo-inverse operator. The SH order $K$ must be chosen according to the level of SNR in the diffusion-weighted data. The higher the order, the more likely the presence of negative peaks in the ODFs resulting from the noise. In Descoteaux et al. (2007), the SH order was empirically set to $K = 4$, leading to $(K+1)(K+2)/2 = 15$ coefficients to be estimated per ODF. Another obvious advantage of the analytical Q-ball model is the drastic reduction of one of the dimension of the reconstruction matrix to an order comparable to that of the DT reconstruction matrix. It is therefore much more suitable for real-time processing.

## 3. Kalman filtering

The Kalman filter is a recursive solver that optimally minimize the mean square error of the estimation (Kalman, 1960). It has been widely used in computer vision dedicated to robotics for estimating the state of a dynamic system from partial and noisy observations (Ayache, 1991; Welch and Bishop, 1991). Because of its recursive nature, it is a suitable method for updating the DTI or analytical QBI model parameters after the acquisition of each new diffusion-sensitized volume. Moreover, the Kalman filter provides, at each time frame, an estimated covariance of the parameter estimate that can be used to automatically stop the ongoing scan when the maximum variance falls below a minimum threshold.

In Section 2, we obtained two general linear models for DTI and QBI of the form $\mathbf{y} = \mathbf{A}\mathbf{x} + \epsilon$. The Kalman filter exploits any new measure $y$ for updating the unknown parameters $\mathbf{x}$, usually called the state vector.

Assume that after the $i$th acquisition, a current estimate $\hat{\mathbf{x}}(i-1)$ is available. Given the new MR measurement $y(i)$ and the vector $\mathbf{a}(i) = [A_{i1},\ldots,A_{iP}]^{\mathrm{T}}$ corresponding to the $i$th row of the matrix $\mathbf{A}$, the innovation $v(i) = y(i) - \mathbf{a}(i)^{\mathrm{T}}\hat{\mathbf{x}}(i-1)$ is calculated. The Kalman filter then updates the parameters using the recursion corresponding to the two prediction and correction steps (11):

$$\begin{aligned} \mathbf{k}(i) &= (1 + \mathbf{a}(i)^{\mathrm{T}}\mathbf{P}(i-1)\mathbf{a}(i))^{-1}\mathbf{P}(i-1)\mathbf{a}(i), \\ \hat{\mathbf{x}}(i) &= \hat{\mathbf{x}}(i-1) + v(i)\mathbf{k}(i), \\ \mathbf{P}(i) &= \mathbf{P}(i-1) - \mathbf{k}(i)\mathbf{a}(i)^{\mathrm{T}}\mathbf{P}(i-1) \end{aligned} \quad (11)$$

where the vector $\mathbf{k}(i)$ is usually called the Kalman gain. $\mathbf{P}(i)$ represents an estimate of the normalized covariance matrix of $\mathbf{x}$ given the information at time $i$. The unnormalized covariance of $\hat{\mathbf{x}}(i)$ is equal to $\hat{\sigma}(i)^2\mathbf{P}(i)$ using the recursion (12):

$$\hat{\sigma}(i) = \frac{i-1}{i}[\hat{\sigma}(i-1) + v(i)^2(1 + \mathbf{a}(i)^{\mathrm{T}}\mathbf{P}(i-1)\mathbf{a}(i))^{-1}] \quad (12)$$

The initial guesses $\hat{\mathbf{x}}(0)$, $\mathbf{P}(0)$ and $\hat{\sigma}(0)$ can be respectively set to the null vector, the identity matrix and zero.

## 4. Optimized diffusion gradient orientation set

Contrary to functional scans where the time order of the stimuli cannot be modified, diffusion scans can play with the set of diffusion gradient orientations in random order, provided it has a uniform distribution of the orientations in the tridimensional space, for obtaining an accurate tensor or Q-ball estimation.

The optimum orientation count is still debated in the literature (Jones, 2004). Increasing this number directly improves the SNR of the ADC, FA and ODF maps, at the price of a longer scan time and knowing that it is not always possible to predict how long a subject will remain still in the magnet. Three different strategies can be followed: the first strategy consists of acquiring only a small uniform set of orientations, during which the patient will probably be quiet; this strategy is likely to prevent any motion problem, but will give poor estimate of the diffusion models as it relies only on a few measurements; the second strategy consist of acquiring a large uniform set of orientations taking a longer time; consequently, the risk of motion is drastically increased and the

acquisition may be stopped before the 3D space is uniformly explored; the third strategy is a compromise between the uniformity of the orientation set and the amount of data required to get a robust estimate of the DT or QBI models; the orientation set is made up of a large number of orientations which are not perfectly uniformly distributed, but whose partial subsets can provide a relatively correct sampling of the 3D orientation space.

We have chosen the third strategy and we have implemented the sequence of orientations proposed in Dubois et al. (2006), which yields the "best" spatial distribution of the orientations, should the acquisition be terminated before completion. We present the design of a set of 42 orientations dedicated to the DT model that has a great clinical impact, but this strategy could also be applied to the QBI model that is less compatible with clinical applications, as it requires longer scans not compatible with restless subjects. The method is inspired from the classical repulsion model of charges distributed on a sphere (Jones et al., 1999; Papadakis et al., 2000) where the orientations are free to pivot and to repulse each other, through electrostatic forces. The equilibrium is reached when the orientations are uniformly distributed, which corresponds to the minimum of the global energy of the system.

Dubois proposed a modified electrostatic model where the repulsive potential $E_{ij}$ between two orientations $\mathbf{o}_i$ and $\mathbf{o}_j$ is of the form $E_{ij} = \alpha_{ij} E^0_{ij}$. $E^0_{ij}$ corresponds to the standard electrostatic-like potential (13). It takes into account the symmetry of the diffusion signal by summing two potentials between the couples of orientations $(\mathbf{o}_i, \mathbf{o}_j)$ and $(\mathbf{o}_i, -\mathbf{o}_j)$ that are equivalent from a physical point of view about the diffusion process. In practice, all the orientations were initially randomized and the global energy minimization was performed using a gradient-descent algorithm,

$$E^0_{ij} = \frac{1}{\|\mathbf{o}_i - \mathbf{o}_j\|} + \frac{1}{\|\mathbf{o}_i + \mathbf{o}_j\|} \tag{13}$$

$$\alpha_{ij} = \alpha^{\frac{s-1}{N_S-1}} \tag{14}$$

The interaction weight $\alpha_{ij}$ was designed such that the whole sequence of 42 orientations consists of a series of smaller meaningful subsets of 14 uniform orientations, while all clusters complement each other with additional orientations (Eq. (14)). The parameter $s$ represents the index of the smallest subset that orientations $\mathbf{o}_i$ and $\mathbf{o}_j$ belong to, and the parameter $N_S$ is total number of subsets. The parameter $\alpha$ represents the minimum interaction weight set to 0.5 in our case. Thus, the more distant in time the orientations are, the more reduced is their interaction. Fig. 1 depicts the interaction weight for any couple of orientations of the optimum 42 orientation set. Thus the orientations 1–14 have a strong interaction, meaning that a high constraint is put on the uniformity of the first subset. The orientations 15–28 have a smaller interaction with other orientations 1–14, meaning that the uniformity constraint is slightly released to let the algorithm converge towards a solution where the orientations 1–28 remain almost uniformly distributed. Last, the orientations 29–42 have an even smaller interaction with orientations 1–28. The uniformity constraint is another time released to enable the convergence of the algorithm, but still sufficient to ensure an almost uniform distribution of 42 orientations.

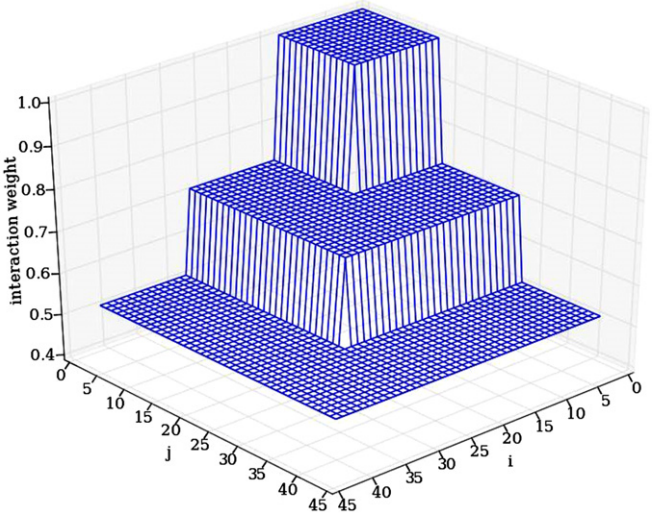


**Fig. 1.** Interaction weights $\alpha_{ij}$ between orientations $i$ and $j$ assuming a set of 42 orientations divided into 3 subsets of 14 orientations; the minimum interaction weight $\alpha$ was set to 0.5; the more distant in time the orientations are, the more reduced is their interaction.

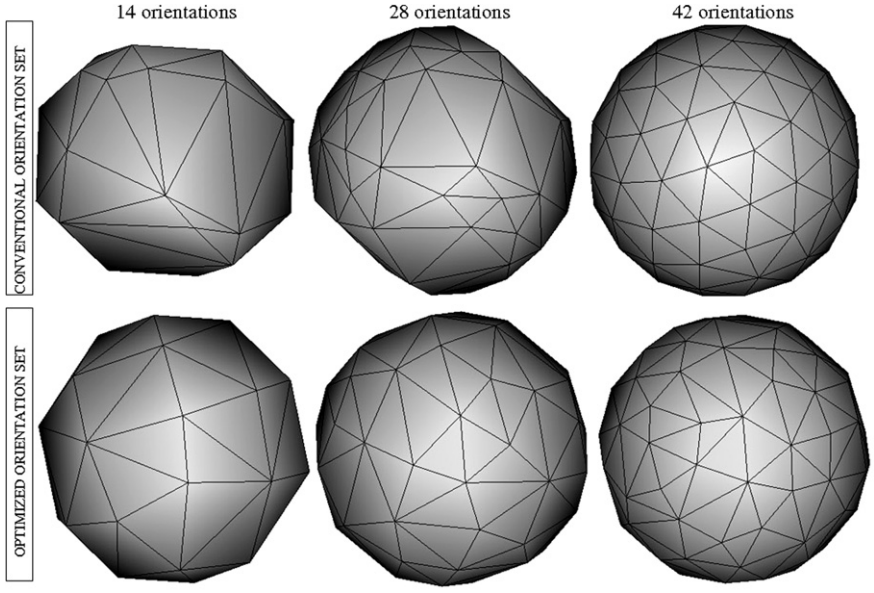


**Fig. 2.** Comparison of conventional and optimized sets of 42 orientations; the surface meshes of the full distributions are represented as well as the surface meshes corresponding to subsets restricted to the 14 or 28 first orientations; the conventional set is more uniform than the optimized set when the full set is acquired, but less uniform when it is incomplete; the optimized set must be employed during real-time scan that can be interrupted at any time.

Using such interaction weights, the first subset of 14 orientations is almost uniformly distributed and corresponds to the minimum number of diffusion orientations to be explored in order to be able to estimate the DT model. Then, if the subject is sufficiently still in the magnet to enable the acquisition of the second subset, the set formed by the 28 orientations is such that the 14 further orientations are complementary to the first 14 orientations, and the distribution of the 28 orientations remains almost uniform on the sphere. The same situation is also true if the signal can be sampled along the 14 orientations of the last subset. At the end, the distributions of 14 and 28 orientations calculated from this method are much more uniform than those obtained from the conventional method, leading to more robust estimates of the DT model, even if the acquisition must be stopped after the acquisition of the first subset. The optimized and conventional full orientation sets remain relatively similar (see Fig. 2) despite the optimized full set is a bit less uniform than the full conventional set.

## 5. Results and discussion

### 5.1. DTI and QBI acquisition settings

The real-time diffusion Kalman filter was evaluated on an adult, under a protocol approved by the Institutional Ethical Committee. The data were acquired on a 1.5 T Signa Excite II MRI system (GE Healthcare, Milwaukee, USA), endowed with a whole body gradient (40 mT/m, 150 T/m/s), a parallel electronic chain with 8 linear channels and an 8-channel receive-only high resolution brain coil antenna coupled with the 1-channel whole body antenna for transmission. A single-shot echo-planar diffusion-weighted spin echo pulse sequence, using a diffusion module based on the twice refocusing technique proposed by Reese et al. (2003) that compensates the Eddy currents to the first order, was used to perform two acquisitions for validating the real-time solvers.

The pulse sequence settings were $b = 700$ s/mm$^2$, 42 optimized gradient orientation set, matrix $128 \times 128$, 60 slice locations, partial Fourier factor of 75%, field of view FOV = 24 cm, slice thickness TH = 2 mm, TE/TR = 66.2 ms/12.5 s for the DTI scan and $b = 3000$ s/mm$^2$, 200 conventional gradient orientation set, matrix $128 \times 128$, 60 slice locations, partial Fourier factor of 75%, field of view FOV = 24 cm, slice thickness TH = 2 mm, TE/TR = 93.2 ms/19 s for the QBI scan. The scan times were 9 min48 s and 72 min50 s, respectively, for the DTI and QBI scans. The SNR of the diffusion-weighted data was equal to 11 at $b = 700$ s/mm2 and equal to 3 at $b = 3000$ s/mm$^2$.

### 5.2. Real-time standard diffusion maps

At each iteration of the DTI scan, an approximation of the diffusion tensor is available for each voxel of the brain using the QBI dedicated Kalman filter (Eq. (2)). Therefore it is possible to process its eigensystem online and then to estimate the ADC/FA/RGB maps. Columns 1–3 of Fig. 3 depict the evolution of these maps during the ongoing scan. For comparison, the 4th column shows the result of a standard offline singular value decomposition. There is no qualitative difference with the 3rd column processed using the Kalman filter.

Fig. 4 shows the evolution of the mean square error between the real-time estimates and the offline estimate according to the iteration index during the scan. The mean square error was plotted for the ADC and the FA indices over the entire brain. The two curves are monotically decreasing to a quasi-null value proving that the Kalman incremental solver can efficiently replace the standard singular value decomposition. The curves also highlight the importance of the order of the orientations: the main slope happens during the acquisition of the first subset of 14 orientations, assessing the quality of the estimate after the first subset and making it exploitable by the clinicians. The decrease of the error is then more moderated, improving progressively the quality of the estimate.

The use of an optimized orientation set speeds up the convergence of the estimation that can be considered exploitable by clinicians from the 14th iteration. The time required to perform one iteration of the DTI Kalman filter over the full brain is less than 8 s on a 3.2 GHz linux station, which is lower than the repetition

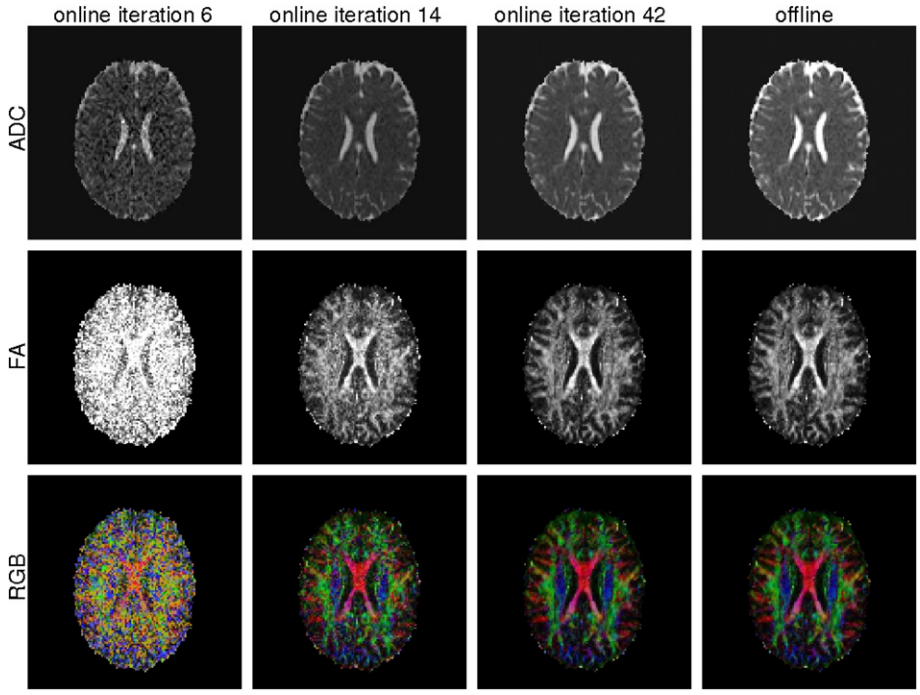


**Fig. 3.** Real-time processing of ADC/FA/RGB maps using the DTI Kalman filter during an ongoing DTI scan at $b = 700$ s/mm$^2$ with 42 diffusion gradient orientations; the columns 1/2/3 correspond to iteration 6, 14 and 42; the last column shows the result of the standard offline processing.

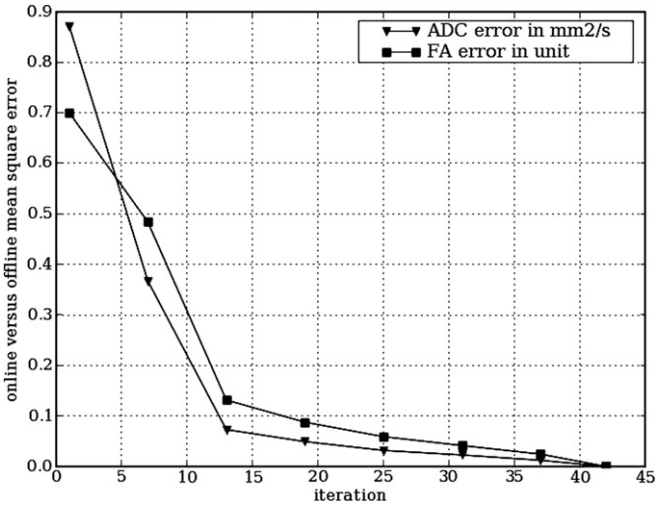


**Fig. 4.** Mean square error between the online estimates of the ADC and the FA and the offline estimate according to the iteration index; the curves highlight the importance of the optimization of the orientation set, depicting main slopes during the acquisition of the first subset of 14 orientations that was built to be almost uniformly distributed.

time TR = 12.5 s of the scan. Consequently, there is no additional delay between two consecutive acquisitions, making this protocol truly real-time.

### 5.3. Real-time orientation distribution function maps

The Q-ball online Kalman filter was used for processing ODFs during the ongoing QBI scan. Contrary to the DTI scan where the orientation set was optimized, the QBI scan was performed with a conventional orientation set. A symmetrical spherical harmonics basis of order 4 was chosen and the Laplace–Beltrami regularization factor was set to 0.006 as proposed in Descoteaux et al. (2006). The choice for the SH order is crucial because using higher SH orders increases the number of SH coefficients to be estimated, and consequently increases the number of iterations of the Kalman filter required to converge. The ODFs are reconstructed along 400 normalized uniform orientations using a normalization for mapping the minimum and maximum values to 0 and 1, respectively, before rendering the shapes of the ODFs. The QBI dedicated Kalman filter (10) provides, at each step and for each voxel of the brain, an estimate of the decomposition of the ODF onto a symmetric spherical harmonics basis from which it is easy to obtain the values for any orientation **o** of the space (Eq. (9)).

The top row in Fig. 5 shows the evolution of the ODF map during the Kalman recursion on a region of interest contained in the subcortical white matter, and exhibiting some fibre crossings as well as voxels with homogeneous fibre populations. At the beginning of the acquisition, the Q-ball renderings depict isotropic ODFs that become progressively anisotropic during the acquisition. As for DTI, there is no qualitative difference between the ODF maps obtained from the online Kalman filter or from the offline Q-ball algorithm given by Eq. (8). However, it is quite interesting to observe that after only half the acquisitions, the ODF shapes are close to their final shapes. This observation is directly linked to the SNR of the diffusion-weighted images that remains low at the current field of 1.5 T for a huge $b$-value of 3000 s/mm$^2$. Increasing the number of measurement points does not necessarily improve the angular resolution of the reconstructed ODFs when the SNR is too poor. This highlights the capability of the online Kalman solver to become a valuable methodological and investigational tool for determining the adequate number of orientations to be used, as well as for setting the adequate voxel size and $b$-value.

Fig. 6 depicts the evolution of the mean square error between the real-time estimate of the SH coefficients and the offline estimate. Three plots shows the evolution of this error for the SH orders 0, 2 and 4 according to the iteration index of the Kalman solver, inside the region of interest specified by the yellow

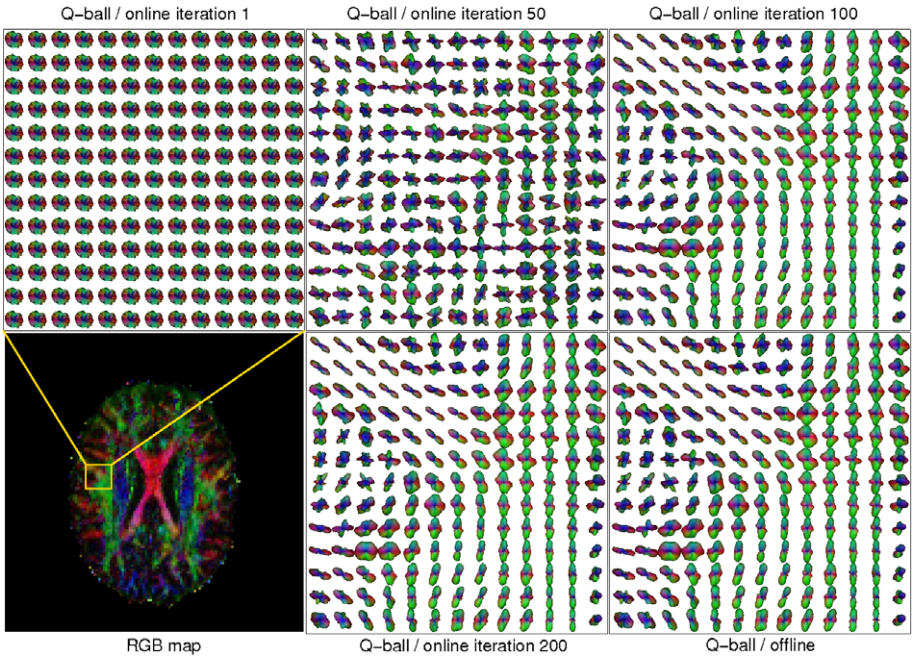


**Fig. 5.** Real-time processing of a Q-ball ODF map using the QBI Kalman filter during an ongoing QBI scan at $b = 3000$ s/mm$^2$ with 200 diffusion gradient orientations; the bottom row displays a direction encoded color map (left) on which is drawn a region of interest inside the white matter, containing fibre crossings and homogeneous voxels, and the corresponding map of Q-ball ODFs (right) processed with the offline routine; the top row and the bottom right shows the iterations 1, 50, 100 and 200 of the same ODF map calculated with the online Kalman filter.

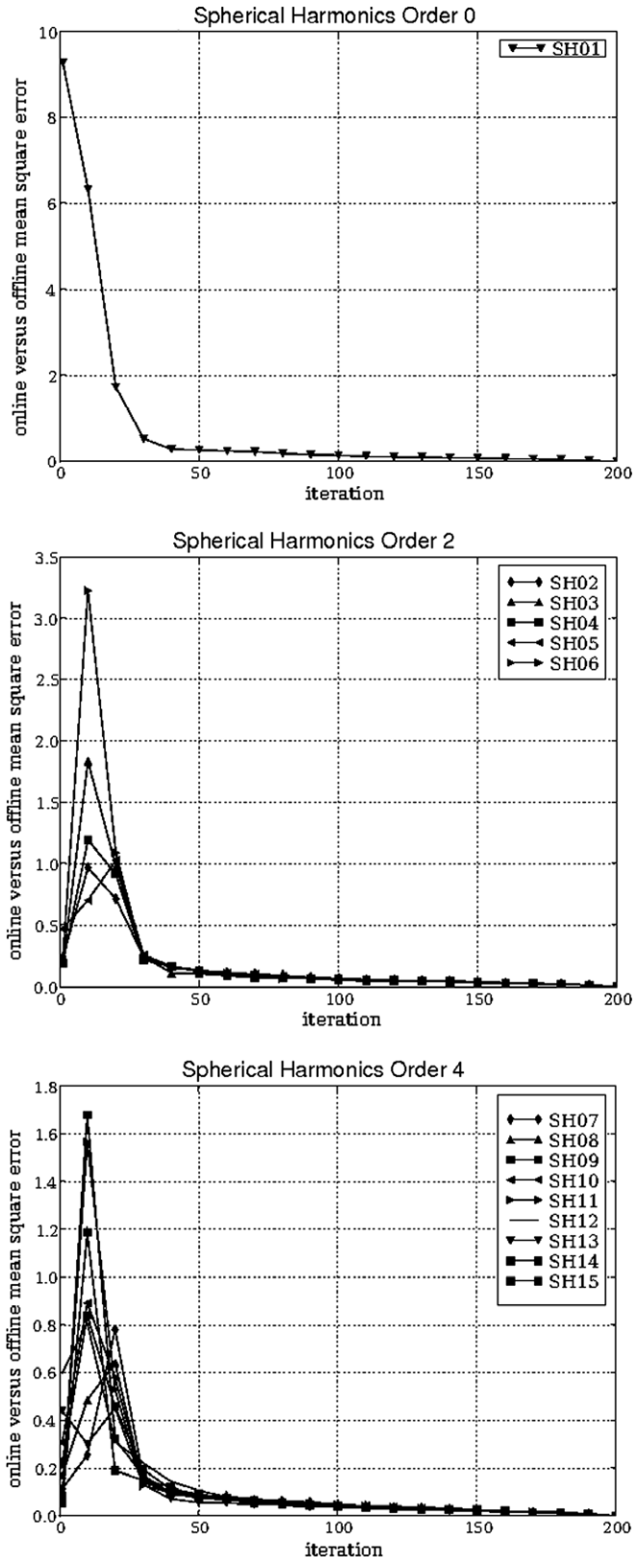


**Fig. 6.** Mean square error between the online estimates of the SH coefficients and the offline estimate according to the iteration index for the SH order $l = 0$ (top, SH01), $l = 2$ (middle, SH02-06) and $l = 4$ (bottom, SH02-15); the error decreases monotically for the zeroth order corresponding to the isotropic diffusion part of the ODF whereas the second and fourth order errors start from a low value, increase during the first 30 iterations, before decreasing and stabilizing continuously; the amplitude orders of the maximum errors is comparable to the magnitude orders of the SH coefficients, i.e. bigger for the second order than for the fourth order.

rectangle in Fig. 5. The error associated to the SH coefficient of order 0 quickly decreases during the first 50 iterations. The behaviour of the errors for the SH order 2 and 4 is quite different: a transition phase occurs during the 30 first iterations where the errors starts with low values, then reach maximum values before decreasing monotically. Due to the use of a conventional orientation set, the mean square error does not depict an initial important slope of the errors, as it would have been the case with an optimized orientation set. That will be investigated in a future study. With the conventional orientation set, the evolution is more continuous and we can see that, after the iteration 100, the SH coefficients remain quite stable. No more orientational information is provided by the following iterations that only improves the estimates in terms of SNR. A question of interest would be determine that minimum number of steps required to estimate the analytical Q-balls. It is probably strongly dependent on the spherical harmonic order. In practice, we have limited the SH order to 4 corresponding to the processing of 15 parameters, and the poor SNR (inferior to 3) lead us to perform at least 100 acquisitions before convergence. In a future study, we will investigate more accurately the relationship between the number of iterations and the SH order.

The time required for performing one iteration of the QBI Kalman filter on a single slice is approximately 1.5 s, which would require 90s to process the entire brain. This processing time exceed the repetition time TR = 19 s of the scan and cannot be performed in true real-time, but only in deferred time. However, we must underline that the time devoted to the processing of the SH decomposition $\mathbf{c}^{\mathrm{ODF}}$ represents no more than 20% of the global processing time. The rest of the time is spent for composing the ODF from the SH coefficients as well as for constructing the triangulated surfaces required for visualization purposes. It is important to say that at this point of the development, the C++ code can still be optimized and will be parallelized in the coming future on a grid of processors in order to be able to process the entire brain in real-time. Moreover, this grid of processors will enable any kind of correction between iterations of the Kalman solver. For instance, a co-registration between the current diffusion-weighted volume and the reference T2 volume could be implemented to correct for motion of the patient at each step of the Kalman filter, and a correction of the susceptibility artefacts could be also implemented if a mapping of the $B_0$ field inhomogeneities is performed before the DTI or QBI acquisition. As we used a single-shot diffusion-weighted echo-planar twice refocusing spin echo sequence for this study, no correction of the Eddy current distortions are needed, because the double refocusing compensates the Eddy currents to the first order, thus providing data without geometric distortions.

## 6. Conclusion

We have developed an incremental Kalman filter-based framework dedicated to real-time diffusion MR imaging. This framework addresses both diffusion tensor and Q-ball models, and enables processing the standard DTI/QBI maps, in real-time during an ongoing scan. The methodology developed in this paper is very suitable for clinical use when a quick feedback is required during the acquisition or when the cooperation of the subject is not certain. More quantitative evaluations of the difference between online and offline reconstructions must be performed for validating this approach, as well as studying more deeply the underlying model of noise present in the QBI data where the SNR is known to be very low (Basu et al., 2006; Landman et al., 2007; Fillard et al., 2007; Assemlal et al., 2007), which was not the main purpose of this paper. This real-time framework seems also to be a promising methodological tool suitable for tuning up the diffusion parameters like the number of orientations, the number of wavevectors

as well as their values (Khachaturian et al., 2007), the regularization factor, and the spherical harmonics order. A future extension of this work entails online fibre tracking. To that end, we plan to modify the diffusion Kalman filter in order to process incremental connectivity maps during ongoing diffusion scans.

## References


Alexander, D.C., 2005. Maximum entropy spherical deconvolution for diffusion MRI. Inform. Process. Med. Imaging 19, 76–87.

Anderson, A.W., 2005. Measurement of fiber orientation distributions using high angular resolution diffusion imaging. Magn. Reson. Med. 54, 1194–1206.

Assaf, Y., Basser, P.J., 2005. Composite hindered and restricted model of diffusion (CHARMED) MR imaging of the human brain. NeuroImage 27 (1), 48–58.

Assemlal, H.E., Tschumperl, D., Brun, L., 2007. Fiber tracking on HARDI data using robust ODF fields. In: Proc. ICIP'2007, IEEE International Conference on Image Processing, San Antonio, USA, September.

Ayache, N., 1991. Artificial Vision for Mobile Robots. The MIT Press, Cambridge, USA.

Basser, P.J., Mattiello, J., LeBihan, D., 1994. Estimation of the effective self-diffusion tensor from the NMR spin echo. J. Magn. Reson. 103, 247–254.

Basu, S., Fletcher, T., Whitaker, R., 2006. Rician noise removal in diffusion tensor. In: Int. Conf. Med. Image Comput. Comput. Assist. Interv., vol. 9, pp. 117–125..

Callaghan, P.T., 1991. Principles of Nuclear Magnetic Resonance Microscopy. Oxford University Press, Oxford.

Deneux, T., Faugeras, O., 2006. EEG-fMRI fusion of non-triggered data using Kalman filtering. In: IEEE International Symposium on Biomedical Imaging.

Descoteaux, M., Angelino, E., Fitzgibbons, S., Deriche, R., 2006. Apparent diffusion coefficients from high angular resolution diffusion images: estimation and applications. Magn. Reson. Med. 56, 395–410.

Descoteaux, M., Angelino, E., Fitzgibbons, S., Deriche, R., 2007. Regularized, fast and robust analytical Q-ball imaging. Magn. Reson. Med. 58, 497–510.

Dubois, J., Poupon, C., Lethimonnier, F., LeBihan, D., 2006. Optimized diffusion gradient orientation schemes for corrupted clinical DTI data sets. MAGMA 19, 134–143.

Fillard, P., Arsigny, V., Pennec, X., Ayache, N., 2007. Clinical DT-MRI estimation, smoothing and fiber tracking with log-Euclidean metrics. IEEE Trans. Med. Imaging 26 (11), 1472–1482.

Frank, L.R., 2002. Characterization of anisotropy in high angular resolution diffusion-weighted MRI. Magn. Reson. Med. 47, 1083–1099.

Hess, C.P., Mukherjee, P., Han, E.T., Xu, D., Vigneron, D.B., 2006. Q-ball reconstruction of multimodal fiber orientations using the spherical harmonic basis. Magn. Reson. Med. 56, 104–117.

Jansons, K.M., Alexander, D.C., 2003. Persistent angular structure: new insights from diffusion magnetic resonance imaging data. Inverse Probl. 19, 1031–1046.

Jian, B., Vemuri, B.C., 2007. Multi-fiber reconstruction from diffusion MRI using mixture of Wisharts and sparse deconvolution. Inform. Process Med. Imaging 20, 384–395.

Jones, D.K., 2004. The effect of gradient sampling schemes on measures derived from diffusion tensor MRI: a Monte Carlo study. Magn. Reson. Med. 51, 807–815.

Jones, D.K.Horsfield, M.A., Simmons, A., 1999. Optimal strategies for measuring diffusion in anisotropic systems by magnetic resonance imaging. Magn. Reson. Med. 42, 515–525.

Kalman, R.E., 1960. A new approach to linear filtering and prediction problems. Trans. ASME – J. Basic Eng. 82 (Series D), 35–45.

Khachaturian, M.-H., Wisco, J.-J., Tuch, D., 2007. Boosting the sampling efficiency of Q-ball imaging using multiple wavevector fusion. Magn. Reson. Med. 57, 289–296.

Landman, B.A., Bazin, P.-L., Prince, J.L., 2007. Diffusion tensor estimation by maximizing Rician likelihood. In: Proc. International Conference on Computer Vision Workshop on Mathematical Methods in Biomedical Image Analysis, Rio de Janeiro, Brazil, October.

LeBihan, D., Breton, E., Lallemand, D., 1986. MR imaging of intravoxel incoherent motions: application to diffusion and perfusion in neurologic disorders. Radiology 161, 401–407.

Liu, C., Bammer, R., Acar, B., Moseley, M., 2004. Characterizing non-Gaussian diffusion by using generalized diffusion tensors. Magn. Reson. Med. 51, 924–937.

Nowak, R.D., 1999. Wavelet-based Rician noise removal for magnetic resonance imaging. IEEE Trans. Image Process. 8 (10), 1408–1419.

Ozarslan, E., Mareci, T.H., 2003. Generalized diffusion tensor imaging and analytical relationships between diffusion tensor imaging and high angular resolution diffusion imaging. Magn. Reson. Med. 50, 955–965.

Ozarslan, E., Shepherd, T.M., Vemuri, B.C., Blackband, S.J., Mareci, T.H., 2006. Resolution of complex tissue microarchitecture using the diffusion orientation transform (DOT). NeuroImage 31 (3), 1086–1103.

Papadakis, N.G., Murrills, C.D., Hall, L.D., Huang, C.L., Carpenter, T.A., 2000. Minimal gradient encoding for robust estimation of diffusion anisotropy. Magn. Reson. Med. 18, 671–679.

Reese, T.G., Weisskoff, R.M., Wedeen, V.J., 2003. Reduction of Eddy-current-induced distortion, in diffusion MRI using a twice-refocused spin echo. Magn. Reson. Med. 49, 177–182.

Roche, A., Pinel, P., Dehaene, S., Poline, J.-B., 2004. Solving incrementally the fitting and detection problems in fMRI time series. In: Proc. Seventh MICCAI, Saint-Malo, France, LNCS, vol. 3217, pp. 719–726.

Sijbers, J., den Dekker, A.J., Scheunders, P., Van Dyck, D., 1998. Maximum-likelihood estimation of Rician distribution parameters. IEEE Trans. Med. Imaging 17 (3), 357–361.

Stejskal, E.O., Tanner, J.E., 1965. Spin diffusion measurements: spin echoes in the presence of a time-dependent field gradient. J. Chem. Phys. 42, 288–292.

Tournier, J.D., Calamante, F., Connelly, A., 2007. Robust determination of the fibre orientation distribution in diffusion MRI: non-negativity constrained super-resolved spherical deconvolution. NeuroImage 35 (4), 1459–1472.

Tuch, D., 2002. Diffusion MRI of complex tissue structure. PhD Thesis, Harvard-MIT.

Tuch, D., 2004. Q-ball imaging. Magn. Reson. Med. 52, 1358–1372.

Wedeen, V.J., Hagmann, P., Tseng, W.Y., Reese, T.G., Weisskoff, R.M., 2005. Mapping complex tissue architecture with diffusion spectrum magnetic resonance imaging. Magn. Reson. Med. 54, 1377–1386.

Welch, G., Bishop, G., 1991. An Introduction to the Kalman filter. In: SIGGRAPH 2001 Course 8, Computer Graphics, Annual Conference on Computer Graphics and Interactive Techniques, Cambridge, USA.

Zhan, W., Gu, H., Xu, S., Silbersweig, D.A., Stern, E., Yang, Y., 2003. Circular spectrum mapping for intravoxel fiber structures based on high angular resolution apparent diffusion coefficients. Magn. Reson. Med. 49, 1077–1088.